THE JOURNAL OF PHYSICAL CHEMISTRY A

Article

pubs.acs.org/JPCA

Valence Electron Ionization Dynamics of Chromium by a Photoelectron Imaging Technique: J^+-Dependent State and Angular Distribution

Jeongmook Lee, Doo-Sik Ahn,† and Sang Kyu Kim*

Department of Chemistry (WCU), KAIST, Daejeon (305-701), Republic of Korea

Supporting Information

ABSTRACT: The photoionization of Cr at excited states is investigated using a velocity-map photoelectron imaging technique. Benzene chromium carbonyl or bis(η^6- benzene) chromium was used as a precursor for the generation of excited Cr atoms. The a $^5S_2 \rightarrow$ x $^5P^\circ_3$ and a $^5D_3 \rightarrow$ y $^5D^\circ_2$ transitions are then employed for the preparation of resonant intermediate states in a two-color two-photon ionization process, in which an electronic configurational change from $3d^4(^5D)4s4p(^1P^\circ)$ to $3d^4 4s(^6D_{J+})$ occurs. The photoelectron kinetic energy distribution is found to be very sensitive to the ionization energy and the total angular momentum quantum number of the chromium ion (J^+). Anisotropy parameters associated with departing electrons also show significant variation depending on the energy and total angular momentum quantum number, suggesting that direct and/or indirect ionization should be quantum-mechanically mixed, manifesting the complicated nature of angular momentum couplings in the ionization continuum.

1. INTRODUCTION

Photoelectron angular distribution (PAD) provides important information about the nature of the quantum states involved in photoionization.[1] For alkali metal atoms, Berry et al. reported a complete study in which an angular momentum coupling model including radial dipole matrix elements and the relative phases of outgoing partial waves was successfully employed.[2−7] Compared to alkali metal[2−4,8] or alkaline earth metal atoms,[5−7] transition metals are intrinsically more complicated in terms of angular momentum coupling, clearly due to the existence of d-subshell electrons. Nonetheless, several beautiful studies have been carried out on several transition metals.[9−12] For instance, Weisshaar et al. reported state-resolved PADs and branching ratios in the two photon ionization of vanadium[11] and iron[12] atoms. They found a strong correlation between the anisotropy parameters and the angular momentum coupling pattern. Several studies on the photoionization of chromium atom are also quite notable.[13−20] Most previous transition metal studies, however, focused on the core−electron ionization process, in which the synchrotron radiation source is mainly used.[16−19] The valence-electron ionization[20] and its photoelectron angular distribution have been less investigated thus far.

Here, we employed a photoelectron velocity-map imaging technique to measure the state-resolved PADs during the two-color two-photon ionization of Cr. For the generation of Cr in the gas phase, we photolyzed the transition metal complexes of benzene chromium carbonyl or bis(η^6- benzene) chromium, as Armentrout et al. had initially employed for the generation of gas-phase metal atoms.[21] The Cr atom is produced in many different quantum states. A specific atomic transition to the x $^5P^\circ_3$ or y $^5D^\circ_2$ state is exclusively selected here for the study of state-resolved ionization dynamics. The chromium cation eigenstates are identified by the kinetic energy of photoelectrons associated with the total angular momentum quantum number, J^+.[10−12] PADs and population branching ratios among J^+ are experimentally determined and their implications are discussed.

2. EXPERIMENT

The detailed experimental setup was described previously.[22] Briefly, BCT (benzene chromium tricarbonyl) or BBC (bis(η^6-benzene) chromium) (Aldrich) was heated to ∼130 °C in a small sample chamber, seeded in the Ar as a carrier gas, and expanded into a vacuum chamber through the orifice of a General Valve (Parker, 0.5 mm diameter) with a backing pressure of ∼2 atm. The molecular beam was skimmed (Beam Dynamics, 2 mm diameter) before it was perpendicularly intersected by two linearly polarized laser beams. The excitation laser (ω_1) was the doubled output of a dye laser (Lumonics, Spectrummaster) pumped by the second harmonic output of a Nd:YAG laser (Continuum, Surelite), whereas the ionization laser (ω_2) was generated by the frequency-doubling of the output of another dye laser (Lamda-Physik, Scanmate II) pumped by another Nd:YAG laser (Spectra-Physics, GCR-150). Two laser pulses were synchronized with the nozzle

Received: September 16, 2012
Revised: February 20, 2013
Published: February 21, 2013

opening at 10 Hz and were spatiotemporally overlapped in counter-propagating manner.

In the two-color two-photon ($\omega_1 + \omega_2$) ionization experiment, the pulse energy of the excitation laser (ω_1) was held below 10 μJ to prevent the one-color two-photon ionization process. The photoelectron signal was practically absent when only one of two laser pulses was applied to the system. The Newton sphere of photoelectrons from the ionization of chromium was accelerated along the time-of-flight axis in the velocity mapping condition and was projected onto a position-sensitive detector equipped with microchannel plates and a P20 phosphor screen (Burle, 3040 FM CT, 40 mm diameter). The light emitted from the phosphor screen was monitored by a photomultiplier tube (PMT) to obtain the frequency-tuned excitation spectra. Images on the phosphor screen were taken by a charge-coupled device (CCD) camera (Sony XC-ST50, 768 × 494 pixels) in conjunction with the IMACQ Megapixel acquisition program developed in the Suits' group.[23] Acquired images were reconstructed and analyzed using the basis-set expansion (BASEX) program.[24]

3. RESULTS AND DISCUSSION

Low-lying excited-state chromium atoms are generated from the multiphoton dissociation of BCT at 298−301 nm (ω_1). The nature of the excited quantum states of Cr is confirmed by photoelectron and photoion spectra taken as a function of the excitation wavelength (ω_1) in the one-color two-photon excitation process (Figure 1). The two spectra are nearly

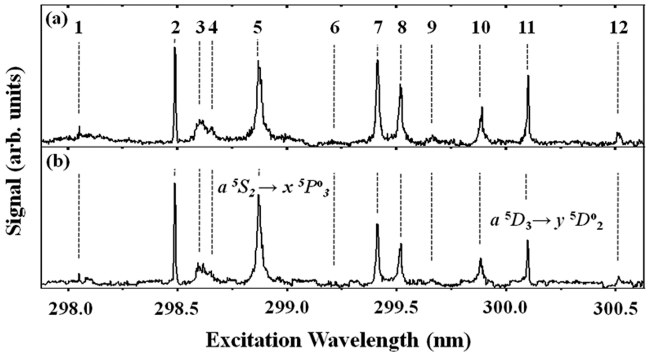

Figure 1. One-color two-photon ionization spectra of a chromium atom: (a) photoion and (b) photoelectron spectrum. More comprehensive assignments of peaks denoted by numbers are given in Table S1 (Supporting Information).

identical to each other, indicating that photoelectrons are dominantly generated from the ionization of the excited chromium atom. Each peak in each spectrum is appropriately assigned on the basis of a comparison to well-established literature values for a number of transitions in Table S1 (Supporting Information). Specifically, atomic transitions of a $^5S_{J''} \rightarrow$ x $^5P^\circ_{J'}$ and a $^5D_{J''} \rightarrow$ y $^5D^\circ_{J'}$ are clearly identified, where J'' and J' are the total angular momentum quantum numbers of the initial and intermediate states, respectively. These transitions are used for the preparation of intermediate states in the subsequent two-color two-photon ionization process, as depicted as a scheme in Figure 2. The ion internal energy ($E_{int,\ ion}$) of chromium is determined from the following energy-conserving relationship.

$$E_{int,ion} = E_{int,neutral} + E_{\omega 1} + E_{\omega 2} - IP - eKE \quad (1)$$

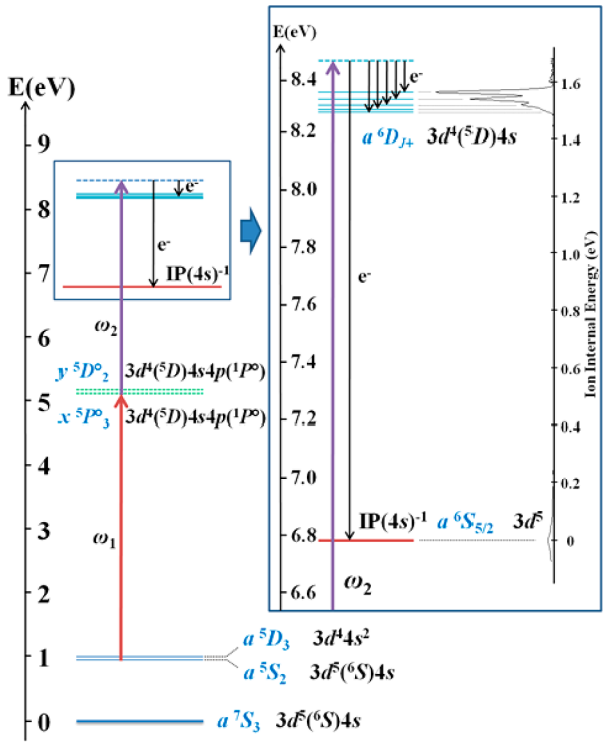

Figure 2. Schematic diagram of the two-color two-photon ionization of a chromium atom. Electronic states and corresponding electron configurations are shown. Excitation of chromium through either the a $^5S_2 \rightarrow$ x $^5P^\circ_3$ or a $^5D_3 \rightarrow$ y $^5D^\circ_2$ transition (ω_1) is followed by photoionization (ω_2) to show the outgoing electron converging to the final cationic state of a $^6D_{J+}$.

Here, $E_{int,neutral}$ is the initial energy of the neutral chromium (a $^5S_2$ or a $^5D_3$), $E_{\omega 1}$ and $E_{\omega 2}$ are the photon energies for the respective excitation and ionization, IP is the ionization potential of chromium (6.7666 eV),[25] and eKE is the kinetic energy of the photoelectron.

Photoelectron images taken by the ($\omega_1 + \omega_2$) ionization via the x $^5P^\circ_3$ or y $^5D^\circ_2$ intermediate states are presented in Figures 3 and 4, respectively. The kinetic energy distributions of photoelectrons associated with the ionization via the x $^5P^\circ_3$ or y $^5D^\circ_2$ intermediate states are also shown with the proper assignments of the Cr^+ quantum states ($^6D_{J+}$), where J^+ is the total angular momentum quantum number of the cation. Term energies associated with the final cationic states were precisely determined from the energetics involved in the ionization via a $^5S_2 \rightarrow$ x $^5P^\circ_3$ and a $^5D_3 \rightarrow$ y $^5D^\circ_2$ transitions (Table S2, Supporting Information). The intermediate state (x $^5P^\circ_3$ or y $^5D^\circ_2$) mainly has the $3d^4 4s4p$ electron configuration (Table S3, Supporting Information),[26] and the core-conserving direct ionization of the $3d^4(^5D)4s4p(^1P^\circ) \rightarrow 3d^4(^5D)4s(^6D_{J+}) + e^-$ process seems to be the dominant ionizing mechanism. Branching ratios among different $^6D_{J+}$ ion states during the ionization process via the x $^5P^\circ_3$ intermediate state are found to vary dramatically with the change of the ionization energy (ω_2), as shown in Figure 3 and Table 1. At an ionization wavelength of 370.78 nm, where the kinetic energy of photoelectron is as high as 0.95 eV, the J^+ distribution is estimated to be approximately 26:18:6:4 for $^6D_{9/2}$:$^6D_{7/2}$:$^6D_{5/2}$:$^6D_{3/2}$. This is at least qualitatively consistent with the statistical expectation of 10:8:6:4 from the ($2J^+ + 1$) degeneracy factor though the $^6D_{9/2}$ and $^6D_{7/2}$ states are ~2.5 times more populated than predicted.

dx.doi.org/10.1021/jp309211b | J. Phys. Chem. A 2013, 117, 2138−2143

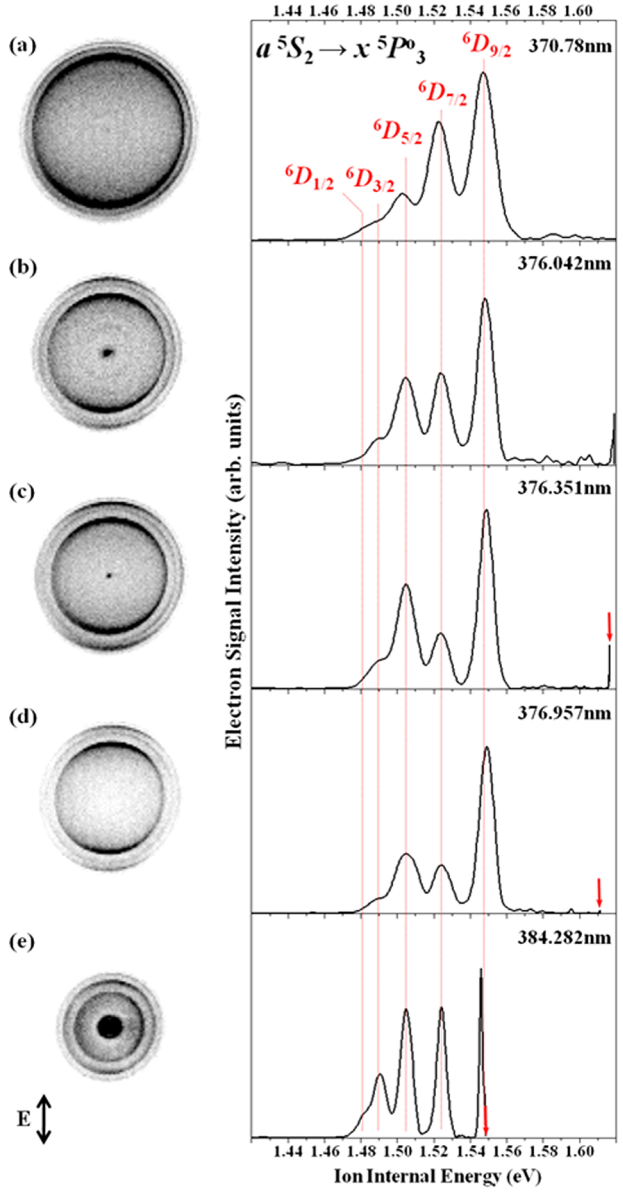

Figure 3. Raw photoelectron images (left) and J^+-state distributions (right) obtained from two-color two-photon ($\omega_1 + \omega_2$) excitation of Cr mediated by the a $^5S_2 \rightarrow$ x $^5P^\circ_3$ transition (ω_1) at ionization wavelengths (ω_2) (a) 370.78, (b) 376.042, (c) 376.351, (d) 376.957, and (e) 384.282 nm. The double-headed arrow shows the polarization axes of the excitation and ionization lasers. The red vertical arrows in the spectra denote the maximum available internal energy at the given level of photon energy.

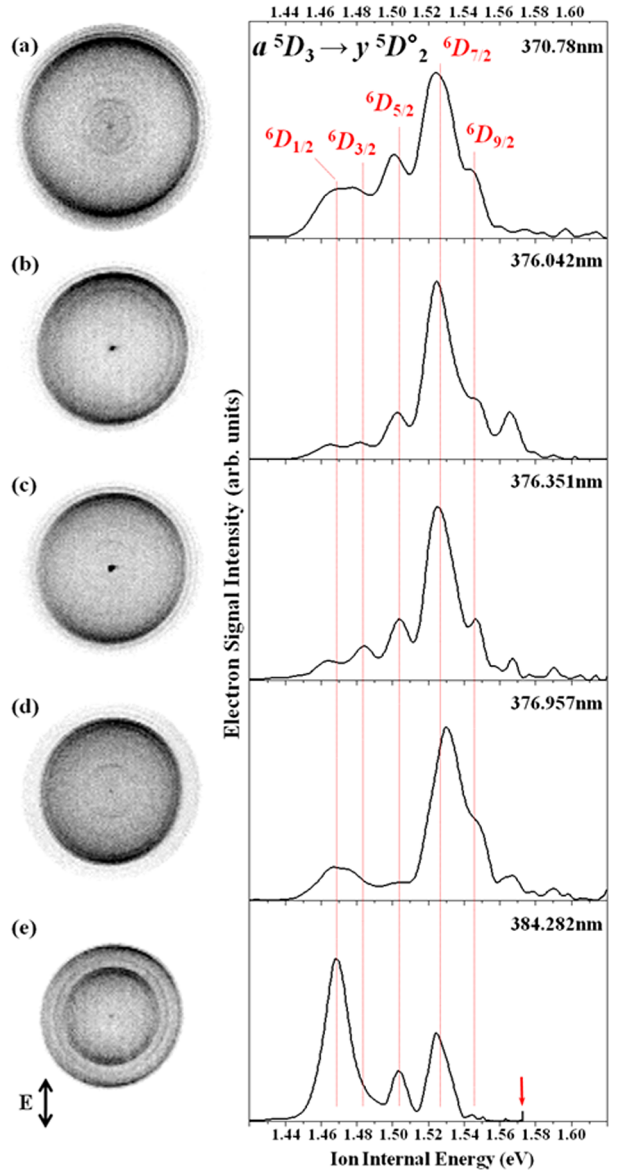

Figure 4. Raw photoelectron images (left) and J^+-state distributions (right) obtained from two-color two-photon ($\omega_1 + \omega_2$) excitation of Cr mediated by the a $^5D_3 \rightarrow$ y $^5D^\circ_2$ transition (ω_1) at ionization wavelengths (ω_2) (a) 370.78, (b) 376.042, (c) 376.351, (d) 376.957, and (e) 384.282 nm. The double-headed arrow shows the polarization axes of the excitation and ionization lasers. The red vertical arrow in the spectra denotes the maximum available internal energy at the given level of photon energy.

A statistical comparison, however, becomes less meaningful at $\omega_2 \sim 376$ nm as the relative ratio of $^6D_{7/2}$ to $^6D_{5/2}$ shows a large fluctuation over a minuscule energy range, as shown in Figure 3b–d. At an ionization wavelength of 384.282 nm, the ionization energy is not sufficient to access all $^6D_{J+}$ ion states. Nonetheless, the fluctuation of the population with J^+ is clearly manifested, as shown in Figure 3e. The J^+-state distribution is found to be quite different for the ionization via the y $^5D^\circ_2$ intermediate state. Specifically, during the photoionization via y $^5D^\circ_2$, the $^6D_{7/2}$ state was found to be most populated at ionization wavelengths of 370.78, 376.042, 376.042, and 376.957 nm, whereas the relative populations among the other $^6D_{J+}$ states at each ionization wavelength were found to

Table 1. Branching Ratios over the Final Ion States from the Ionization of Chromium Using the Transition of a $^5S_2 \rightarrow$ x $^5P^\circ_3$

excitation wavelength (nm)	ionization wavelength (nm)	final ion-state distribution (%)				
		$^6D_{9/2}$	$^6D_{7/2}$	$^6D_{5/2}$	$^6D_{3/2}$	$^6D_{1/2}$
298.868	370.78	48.3	34.0	10.3	7.4	~0
	376.042	41.6	25.9	25.7	6.8	~0
a $^5S_2 \rightarrow$ x $^5P^\circ_3$	376.351	46.1	16.4	31.2	6.3	~0
	376.957	49.8	17.9	28.3	4.0	~0

dx.doi.org/10.1021/jp309211b | J. Phys. Chem. A 2013, 117, 2138–2143

be quite different. Interestingly, at ω_2 = 384.282 nm, the $^6D_{1/2}$-state population is most pronounced whereas the $^6D_{9/2}$ state was almost completely diminished, as shown in Figure 4e. The experimental finding that the J^+-state distribution is highly sensitive to the ionization energy strongly indicates that phases of partial waves may interfere to result in a complicated intensity pattern in the photoelectron spectrum.

As expected from the energy-dependent variation of the J^+-state distribution, the photoelectron angular distribution (PAD) also shows dramatic variations depending on the $^6D_{J+}$ state of the chromium ion. Generally, PAD for two-photon ionization using the linearly polarized light is described by the following equation.[27−29]

$$I(\theta) = \frac{\sigma}{4\pi}[1 + \beta_2 P_2(\cos\theta) + \beta_4 P_4(\cos\theta)] \quad (2)$$

Here, θ is the angle between the direction of the outgoing electron and the electric vector of the linearly polarized light, σ is the total ionization cross section, $P_2(\cos\theta)$ and $P_4(\cos\theta)$ are respectively the second and fourth Legendre polynomials, and β_k is the anisotropy parameter. In Figures 5 and 6, PADs

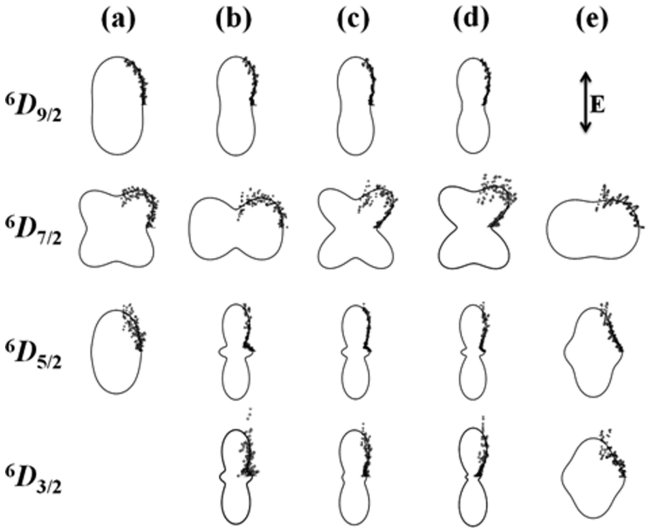

Figure 5. Polar plots of photoelectrons associated with different J^+ states of a chromium ion at various ionization wavelengths of (a) 370.78, (b) 376.042, (c) 376.351, (d) 376.957, and (e) 384.282 nm during two-color two-photon ionization via the x $^5P°_3$ intermediate state. The polarization axes of the ionization and excitation laser pulses are both vertical. The solid lines are fits to the experiment results (dots) from eq 2 with the β_2 and β_4 values listed in Table 2.

extracted from the photoelectron images are plotted in the polar coordinate with the corresponding fits using eq 2 with the β_2 and β_4 values listed in Table 2. Generally, PADs from the ionization via the x $^5P°_3$ result in large positive β_2 and β_4 values as the ionization converges to the $^6D_{9/2}$, $^6D_{5/2}$, or $^6D_{3/2}$ state whereas PAD associated with $^6D_{7/2}$ gives smaller positive β_2 and negative β_4 values. Large β_4 values observed in PADs from the x $^5P°_3$ (L = 1) intermediate state simply imply that the d-partial wave is heavily involved in the outgoing electron wave function. The relative phase of the s- and d- partial waves of the departing electron, according to the $\Delta l = \pm 1$ selection rule,[2] therefore strongly depends on the final quantum state of the cation. PAD shows a large fluctuation of anisotropy parameters also with the change of the ionization energy, as clearly shown in Figure 5. During ionization via the y $^5D°_2$ state, on the other

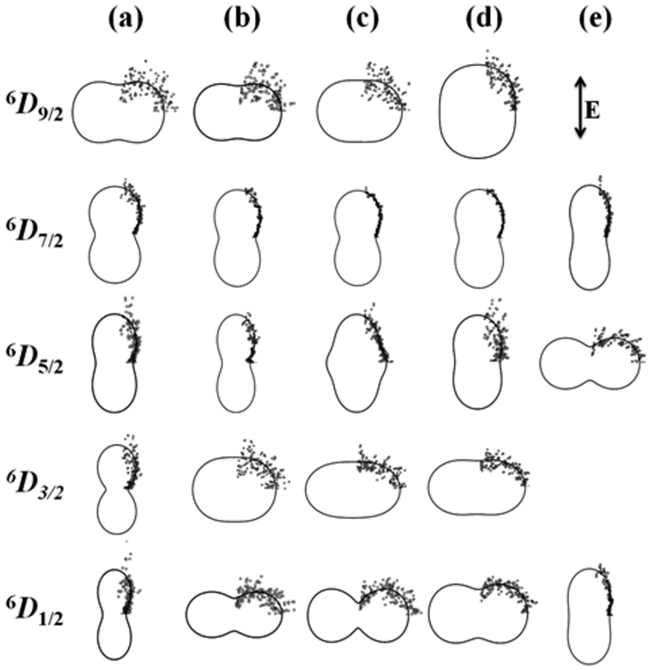

Figure 6. Polar plots of photoelectrons associated with different J^+ states of a chromium ion at various ionization wavelengths of (a) 370.78, (b) 376.042, (c) 376.351, (d) 376.957, and (e) 384.282 nm during two-color two-photon ionization via the y $^5D°_2$ intermediate state. The polarization axes of the ionization and excitation laser pulses are both vertical. The solid lines are fits to the experiment results (dots) from eq 2 with the β_2 and β_4 values listed in Table 2.

hand, PADs give very small β_4 values for all J^+-states, indicating that the p-partial wave is dominant for the outgoing electron, which is again consistent with the $\Delta l = \pm 1$ selection rule, as p and f partial waves are expected from the y $^5D°_2$ state (L = 2). A large fluctuation of β_2 is also observed as a function of the ionization energy, as shown in Figure 6. It is noteworthy that β_2 becomes negative for photoelectrons associated with $^6D_{3/2}$ or $^6D_{1/2}$ at several ionization wavelengths. This, presumably results from the destructive interferences of partial waves with respect to the polarization vector axis, as observed for PAD from the oxygen anion.[30,31]

It appears to be a formidable task to determine the ionization dynamics of Cr fully, as the electronic structure of the transition metal and interferences among many different partial waves are highly complicated due to the strong spin−orbit coupling. Electronic configurational mixing is one of the obstacles to understanding the interference mechanism acting during ionization process. For instance, the electronic characteristics of the x $^5P°_3$ or y $^5D°_2$ are scarcely described by the zeroth-order electronic configuration. The x $^5P°_3$ state consists of ∼55% of $3d^4(^5D)4s4p(^1P°)$[26] and ∼8% of $3d^5(^4P)4p$ configurations, whereas the remaining 37% is not yet characterized.[26] Similarly, the y $^5D°_2$ state is regarded as a mixture of ∼56% of $3d^4(^5D)4s4p(^1P°)$ and ∼13% of $3d^5(^4P)4p$ configurations.[26] A quantitative understanding of the Cr photoionization dynamics thus requires multichannel quantum defect (MCQT) calculations based on a more comprehensive characterization of the quantum states involved in the optical excitation and ionization processed. In this report, we have not attempted theoretical calculations.

dx.doi.org/10.1021/jp309211b | J. Phys. Chem. A 2013, 117, 2138−2143

Table 2. Anisotropy Parameters (β_2,β_4) Used for Fitting the Photoelectron Angular Distributions from the Ionization of Excited-State Chromium via the Atomic Transitions of a $^5S_2 \rightarrow x\ ^5P^\circ_3$ and a $^5D_3 \rightarrow y\ ^5D^\circ_2$[a]

		final ion state											
		$^6D_{9/2}$		$^6D_{7/2}$		$^6D_{5/2}$		$^6D_{3/2}$		$^6D_{1/2}$			
excitation λ (nm)	ionization λ (nm)	β_2	β_4	β_2	β_4	β_2	β_4	β_2	β_4	β_2	β_4		
298.868	370.780	0.47 (6)	0.06 (8)	0.26 (9)	0.37 (6)	0.35 (7)	0.09 (5)						
	376.042	0.84 (10)	0.25 (8)	−0.34 (9)	−0.21 (7)	0.78 (5)	0.91 (5)	0.81 (16)	0.73 (21)				
	376.351	0.89 (9)	0.28 (7)	0.40 (5)	−0.62 (3)	0.96 (8)	0.89 (6)	1.08 (8)	0.62 (6)				
a $^5S_2 \rightarrow x\ ^5P^\circ_3$	376.957	1.10 (6)	0.41 (5)	0.59 (13)	−0.56 (7)	1.19 (10)	1.08 (8)	1.69 (12)	1.06 (11)				
	384.282			−0.28 (10)	−0.06 (5)	0.23 (6)	0.30 (15)	0.11 (6)	0.19 (5)				
300.102	370.780	−0.26 (12)	−0.09 (9)	0.65 (6)	−0.06 (7)	0.70 (13)	0.10 (9)	1.01 (13)	0.03 (13)	1.10 (11)	0.27 (8)		
	376.042	−0.27 (13)	−0.06 (6)	0.70 (7)	0.04 (6)	0.94 (8)	0.22 (6)	−0.15 (9)	−0.03 (7)	−0.56 (14)	0.01 (14)		
	376.351	−0.19 (15)	−0.03 (12)	0.70 (6)	0.02 (5)	0.31 (5)	0.21 (8)	−0.34 (9)	0.04 (11)	−0.56 (6)	−0.14 (19)		
a $^5D_3 \rightarrow y\ ^5D^\circ_2$	376.957	0.16 (7)	−0.05 (4)	0.65 (5)	0.03 (5)	0.53 (12)	0.04 (13)	−0.36 (7)	0.02 (7)	−0.36 (5)	−0.08 (6)		
	384.282			0.84 (6)	0.25 (10)	−0.52 (6)	−0.06 (5)			0.61 (2)	0.13 (7)		

[a]Values in parentheses given here are the standard deviations from independent analyses of the four quadrants of the same image in the last digits.

4. CONCLUSION

Excited chromium atoms are generated by the photolysis of benzene chromium carbonyl or bis(η^6- benzene)chromium at 298−301 nm. Atomic transitions a $^5S_2 \rightarrow x\ ^5P^\circ_3$ and a $^5D_3 \rightarrow y\ ^5D^\circ_2$ are employed to prepare specific intermediate states during the two-color two-photon ionization of Cr. The photoelectron kinetic energy and angular distributions associated with the final chromium cationic states are obtained by a velocity-map imaging technique. The ionization dynamics vary quite dramatically as the total ionization energy changes in terms of the intensity distributions among different J^+ states at the final $^6D_{J+}$ level and in terms of the phase differences of the outgoing partial waves, resulting in large fluctuations of β_2 and β_4 values over a small ionization energy range. Furthermore, the ionization processes via the $x\ ^5P^\circ_3$ and $y\ ^5D^\circ_2$ intermediate states are very different in terms of the J^+-dependent state and angular distributions. This experimental work, although it lacks a rigorous theoretical analysis, provides important information for regarding our understanding of the complex ionization dynamics of transition metals in the gas phase.

■ ASSOCIATED CONTENT

Ⓢ Supporting Information

Tables summarizing the assignments of each peak in photoion spectrum in Figure 1, observed ion internal energy of final ion states from each ionization process, and electronic configurations, term symbols, energy levels, and leading percentage of each state. This information is available free of charge via the Internet at http://pubs.acs.org

■ AUTHOR INFORMATION

Corresponding Author

*Fax: (+) 82-42-350-2810. Tel: (+)82-42-350-2843. E-mail: sangkyukim@kaist.ac.kr.

Present Address

†Fritz-Haber-Institut der Max-Planck-Gesellschaft, Berlin, Germany.

Notes

The authors declare no competing financial interest.

■ ACKNOWLEDGMENTS

This work was supported by the National Research Foundation (2012-0005607) and by the WCU program (R31-10071). The support from the center for space-time molecular dynamics (2012-0000779) is also appreciated.

■ REFERENCES

(1) Reid, K. L. *Annu. Rev. Phys. Chem.* **2003**, *54*, 397−424.
(2) Chien, R.; Mullins, O. C.; Berry, R. S. *Phys. Rev. A* **1983**, *28*, 2078−2084.
(3) Strand, M. P.; Hansen, J.; Chien, R.-L.; Berry, R. S. *Chem. Phys. Lett.* **1978**, *59*, 205−209.
(4) Hansen, J. C.; Duncanson, J. A., Jr.; Chien, R.-L.; Berry, R. S. *Phys. Rev. A* **1980**, *21*, 222−233.
(5) Mullins, O. C.; Chien, R.-L.; Hunter, J. E., III; Keller, J. S.; Berry, R. S. *Phys. Rev. A* **1985**, *31*, 321−328.
(6) Mullins, O. C.; Chien, R.-L.; Hunter, J. E., III; Jordon, D. K.; Berry, R. S. *Phys. Rev. A* **1985**, *31*, 3059−3067.
(7) Hunter, J. E., III; Keller, J. S.; Berry, R. S. *Phys. Rev. A* **1986**, *33*, 3138−3145.
(8) Compton, R. N.; Stockdale, J. A. D.; Cooper, C. D.; Tang, X.; Lambropoulos, P. *Phys. Rev. A* **1984**, *30*, 1766−1774.

(9) Edelstein, S.; Lambropoulos, M.; Duncanson, J.; Berry, R. S. *Phys. Rev. A* **1974**, *9*, 2459−2465.
(10) Sanders, L.; Sappey, A. D.; Weisshaar, J. C. *J. Chem. Phys.* **1986**, *85*, 6952−6963.
(11) Sanders, L.; Hanton, S. D.; Weisshaar, J. C. *J. Chem. Phys.* **1990**, *92*, 3485−3497.
(12) Hanton, S. D.; Noll, R. J.; Weisshaar, J. C. *J. Chem. Phys.* **1992**, *96*, 5165−5175.
(13) Williams, M. W.; Beekman, D. W.; Swan, J. B.; Arakawa, E. T. *Anal. Chem.* **1984**, *56*, 1348−1350.
(14) Sonntag, B.; Zimmermann, P. *Rep. Prog. Phys.* **1992**, *55*, 911−987.
(15) Arp, U.; Iemura, K.; Kutluk, G.; Nagata, T.; Yagi, S.; Yagishita, A. *J. Phys. B: At. Mol. Opt. Phys.* **1995**, *28*, 225−232.
(16) Dohrmann, Th.; von dem Borne, A.; Verweyen, A.; Sonntag, B.; Wedowski, M.; Godehusen, K.; Zimmermann, P.; Dolmatov, V. K. *J. Phys. B: At. Mol. Opt. Phys.* **1996**, *29*, 4641−4658.
(17) von dem Borne, A.; Johnson, R. L.; Sonntag, B.; Talkenberg, M.; Verweyen, A.; Wernet, Ph.; Schulz, J.; Tiedtke, K.; Gerth, Ch.; Obst, B.; Zimmerman, P.; Hansen, J. *Phys. Rev. A* **2000**, *62*, 052703.
(18) Godehusen, K.; Wernet, P.; Richter, T.; Zimmermann, P.; Martins, M. *Phys. Rev. A* **2003**, *68*, 052707.
(19) Whitfield, S. B.; Krosschell, B. D.; Wehlitz, R. *J. Phys. B: At. Mol. Opt. Phys.* **2004**, *37*, 3435−3455.
(20) Dyke, J. M.; Fayad, N. K.; Morris, A.; Trickle, I. R. *J. Phys. B: At. Mol. Phys.* **1979**, *12*, 2985−2991.
(21) Niles, S.; Prinslow, D. A.; Wight, C. A.; Armentrout, P. B. *J. Chem. Phys.* **1990**, *93*, 6186−6199.
(22) Lee, K. S.; Lim, J. S.; Ahn, D. S.; Choi, K. W.; Kim, S. K. *J. Chem. Phys.* **2006**, *124*, 124307.
(23) Li, W.; Chambreau, S. D.; Lahankar, S. A.; Suits, A. G. *Rev. Sci. Instrum.* **2005**, *76*, 063106.
(24) Dribinski, V.; Ossadtchi, A.; Mandelshtam, V. A.; Reisler, H. *Rev. Sci. Instrum.* **2002**, *73*, 2634−2642.
(25) Sugar, J.; Corliss, C. *J. Phys. Chem. Ref. Data* **1985**, *14* (Suppl. 2), 1−664.
(26) Sugar, J.; Corliss, C. *J. Phys. Chem. Ref. Data* **1977**, *6*, 317−383.
(27) Lambropoulos, P. *Adv. At. Mol. Phys.* **1976**, *12*, 87−164.
(28) Cooper, J.; Zare, R. N. *Lectures in Theoretical Physics*; Geltman, S., Mahanthappa, K. T., Brittin, W. E., Eds.; Gordon and Breach: New York, 1969; Vol. *XIC*.
(29) Suzuki, T.; Whitaker, B. J. *Int. Rev. Phys. Chem.* **2001**, *20*, 313−356.
(30) Hall, J. L.; Siegel, M. W. *J. Chem. Phys.* **1968**, *48*, 943−945.
(31) Cooper, J.; Zare, R. N. *J. Chem. Phys.* **1968**, *48*, 942−943.